Radio Science, Volume 33, Number 1, Pages 175–190, January–February 1998

Ionospheric electron density profiles obtained with the Global Positioning System: Results from the GPS/MET experiment

George A. Hajj and Larry J. Romans

Jet Propulsion Laboratory, California Institute of Technology, Pasadena

Abstract. The Global Positioning System Meteorology (GPS/MET) experiment, which placed a GPS receiver in a low-Earth orbit tracking GPS satellites setting behind the Earth's limb, has collected data from several thousands of occultations since its launch in April 1995. This experiment demonstrated for the first time the use of GPS in obtaining profiles of electron density and other geophysical variables such as temperature, pressure, and water vapor in the lower atmosphere. This paper discusses some of the effects of the ionosphere, such as bending and scintillation, on the GPS signal during occultation. It also presents a set of ionospheric profiles obtained from GPS/MET using the Abel inversion technique, and compares these profiles with ones obtained from the parameterized ionospheric model (PIM) and with ionosonde and incoherent scatter radar measurements. Statistical comparison of N_mF_2 values obtained from GPS/MET profiles and nearby ionosondes indicates that they agree to about ~20% (1-sigma) in a fractional sense. The high vertical resolution, characteristic of the occultation geometry, is reflected in the GPS/MET profiles which reveal ionospheric structures of very small vertical scales such as the sporadic *E*.

1. Introduction

When a signal transmitted by a Global Positioning System (GPS) satellite and received by a low-Earth orbit (LEO) satellite passes through the Earth's atmosphere in a limb sounding geometry (Figure 1), its phase and amplitude are affected in ways that are characteristic of the index of refraction of the medium along the path of propagation. By applying certain assumptions on the variability of the index of refraction of the propagating media (e.g., spherical symmetry in the locality of the occultation), phase change measurements between the transmitter and the receiver yield refractivity profiles in the ionosphere (~60-1000 km) and lower neutral atmosphere (0-60 km). The refractivity, in turn, yields electron density in the ionosphere, temperature and pressure in the neutral stratosphere and upper troposphere; and (with the aid of independent temperature data) water vapor density in the lower troposphere.

This method has been applied repeatedly in NASA's planetary occultation experiments [see, e.g., *Fjeldbo et al.*, 1971; *Tyler*, 1987] and was inherited from the area of geological mapping of the Earth's interior. However, the application of the technique to sense the Earth's neutral atmosphere or ionosphere had to await the development of an infrastructure built for completely different purposes, namely, the set of 24 GPS satellites launched and maintained by the Department of Defense for the purpose of navigation. Once this set of satellites became operational, it became clear to some [e.g., *Yunck et al.*, 1988; *Gurvich and Krasil'nikova*, 1990] that placing one receiver in LEO, with a full 360^0 field of view of the Earth's limb, will provide about 500 globally distributed occultations daily at a very low cost. This concept was tested for the first time with the GPS Meteorology (GPS/MET) experiment which placed a GPS receiver in LEO. The

Paper number 97RS03183.
0048-6604/98/97RS-03183$11.00

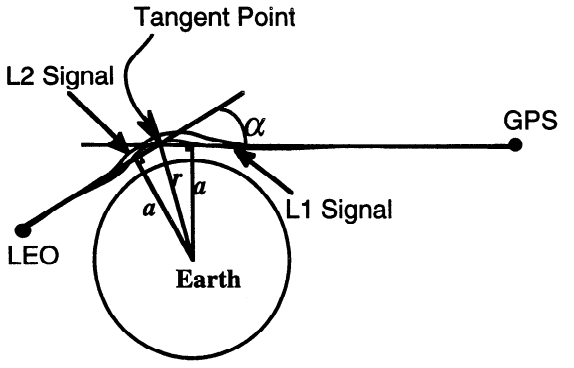

Figure 1. Occultation geometry defining *a*, *r*, α and the tangent point and showing the separation of the L1 and L2 signals due to the dispersive ionosphere.

GPS/MET experiment, managed by the University Corporation for Atmospheric Research (UCAR) [*Ware et al.*, 1996], consisted of a 2-kg GPS receiver piggybacked on the MicroLab I satellite which has a circular orbit of 740-km altitude and 70° inclination. The GPS receiver is a space qualified TurboRogue [*Meehan et al.*, 1992] capable of tracking up to eight GPS satellites simultaneously at both frequencies transmitted by GPS. Owing to the limited field of view of the GPS receiver's antenna and the onboard memory limitation of the satellite, the GPS/MET collects anywhere between 100 and 200 globally distributed occultations daily. Since the start of the GPS/MET experiment in April of 1995, tens of thousands of occultations have been recorded by GPS/MET, providing a very rich data set to study the ionosphere and the lower neutral atmosphere.

Owing to the abundance of neutral atmospheric data from radiosondes and the existence of accurate numerical weather models, several studies that examine the accuracies of temperature and pressure profiles obtain from GPS/MET have been published. For example, *Kursinski et al.* [1996] and *Ware et al.* [1996] demonstrated that GPS/MET temperature profiles are accurate to better than 1-2° K between ~5 and 30 altitudes, while *Leroy* [1997] showed that geopotential heights of pressure levels in the same region are accurate to better than 20 m. In the ionosphere, on the other hand, owing to the sparsity of data, comparisons have been somewhat limited. In order to assess the accuracy of ionospheric electron densities derived from GPS occultations, several investigators have performed simulated experiments where synthetic data based on ionospheric models have been created and then inverted [see, e.g., *Hajj et al.*, 1994; *Høeg et al.*, 1995; *Decker et al.*, 1996; *Leitinger et al.*, 1997]. These studies suggested several possible ways of inverting total electron content (TEC) data obtained from GPS occultations, starting from the simplest approach of assuming a spherically symmetric medium and solving for an electron density profile for each occultation (e.g., the Abel inversion approach presented below), to combining different occultations along with ground data to obtain two-dimensional (2-D) or 3-D images of the ionosphere (tomographic inversions). While it is obvious that the assumption of spherical symmetry in the ionosphere is never an accurate one, the Abel inversion approach serves well as a starting point to understand some of the unique features associated with GPS occultation data. The purpose of this paper is to examine some of these features and to estimate the accuracy of retrieved electron density profiles obtained with the Abel inversion by comparing them with other independent measurements such as incoherent scatter radar and ionosondes. The accuracy obtained with this approach will be a lower bound on what can be achieved with more elaborate inversion methods.

The outline of the paper is as follows. Section 2 will briefly explain the Abel inversion technique as applicable to the ionosphere. Section 3 will examine some of the effects of the ionosphere on occulted signals, including bending and scintillation. Section 4 will present some electron density profiles derived from GPS/MET, the GPS/MET ionospheric coverage, and some comparisons to ionospheric models and to ionospheric measurements from incoherent scatter radars and ionosondes. Some conclusions are discussed in section 5.

2. Radio Occultation Technique: The Abel Inversion

The basic observable for each occultation is the phase change between the transmitter and the receiver as the signal propagates through the ionosphere and the neutral atmosphere (Figure 1). A GPS phase measurement can be modeled as

$$\Phi = \rho + B^{\text{trans}} - B^{\text{rec}} + \Delta^{\text{neutral}} + \Delta^{\text{iono}} + b, \quad (1)$$

where ρ is the geometrical range; B^{trans} and B^{rec} are clock biases for the transmitter and the receiver, respectively; Δ^{neutral} and Δ^{iono} are the delays due to the neutral atmosphere and the ionosphere; and b is a phase ambiguity. In addition to the occulting GPS and LEO satellites, other measurements, taken from a network of

ground receivers tracking GPS and from the LEO tracking other GPS satellites, are used to obtain precise orbit and clock solutions of the satellites. The details of how the GPS/MET signal is calibrated in order to isolate the atmospheric effects on the occulted signals are given elsewhere [*Hajj et al.*, 1995]. Here it suffices to say that through the calibration process the sum of the neutral and the ionospheric delays is isolated (up to a constant). When the tangent point of the occulted link is in the ionosphere, delay due to the neutral atmosphere is negligible. It is important to point out the difference between this processing technique for extracting ionospheric delay which makes use of a single frequency and the traditional method of measuring TEC which is obtained from a linear combination of the GPS dual frequencies. While the former technique results in less noisy determination of ionospheric delay, especially when anti-spoofing (AS) is on, the latter is simpler because it does not require accurate calibration of clocks and orbit errors which cancel when forming the L1 and L2 linear combination. On the other hand, the latter approach assumes that the L1 and L2 signals travel along the same raypath in the ionosphere, an assumption which breaks down when the signals are bent sufficiently during occultation by the ionosphere. This issue will be discussed further below. The results presented throught this paper are based on measurements of the L1 frequency, unless it is stated otherwise.

When the ionospheric delay is determined, it is differentiated (after proper smoothing) to obtain the extra Doppler shift induced by the medium. This extra Doppler shift can be used to derive the bending of the signal, α, as a function of the asymptote miss distance, a (Figure 1), by assuming a spherically symmetric atmosphere in the locality of the occultation; the relationship between the direction of the signal's propagation and the extra Doppler shift, Δf, is then given by

$$\Delta f = \frac{f}{c}\left[\mathbf{v}_t.\mathbf{k}_t - \mathbf{v}_r.\mathbf{k}_r - (\mathbf{v}_t - \mathbf{v}_r).\mathbf{k}\right], \qquad (2)$$

where f is the operating frequency; c is the speed of light; $\mathbf{v}_t$ and $\mathbf{v}_r$ are the transmitter and receiver velocity, respectively; $\mathbf{k}_t$ and $\mathbf{k}_r$ are the unit vectors in the direction of the transmitted and received signal, respectively; and $\mathbf{k}$ is the unit vector in the direction of the straight line connecting the transmitter to the receiver. Assuming spherical symmetry introduces the extra constraint

$$a = n(\mathbf{r}_t)\left\|\mathbf{r}_t \times \mathbf{k}_t\right\| = n(\mathbf{r}_r)\left\|\mathbf{r}_r \times \mathbf{k}_r\right\|, \qquad (3)$$

where $\mathbf{r}_t$ and $\mathbf{r}_r$ are the coordinates of the transmitter and the receiver, respectively; and n is the index of refraction at the specified coordinate. Equations (2) and (3) can be solved simultaneously in order to estimate the total atmospheric bending. Solving these two equations ideally requires knowledge of n at the satellites locations; however, in the appendix we estimate that by setting n=1 at the transmitter or the receiver (when the receiver is at reasonably high altitude, such as the case for the GPS/MET experiment), the solved-for ionospheric bending and the corresponding electron density are overestimated by no more than 0.5% of their true values. We proceed therefore by setting $n(\mathbf{r}_t) = n(\mathbf{r}_r) = 1$.

The spherical symmetry assumption can also be used to relate the signal's bending to the medium's index of refraction, n, via the relation [*Born and Wolf*, 1980, p. 123]

$$\alpha(a) = -2a\int_a^\infty \frac{1}{\sqrt{a'^2 - a^2}}\frac{d\ln(n)}{da'}da', \qquad (4)$$

where $a = nr$ and r is the radius of the tangent point (Figure 1). This integral equation can then be inverted by using an Abel integral transform given by [see, e.g., *Tricomi*, 1985, p. 39]

$$\ln(n(a)) = -\frac{1}{\pi}\int_a^\infty \frac{\alpha(a')}{\sqrt{a'^2 - a^2}}da'. \qquad (5a)$$

The upper limit of the integral in equation (5) requires knowledge of the bending as a function of a all the way up to the top of the ionosphere. The GPS is above most of the ionosphere; however, this is not true of the GPS/MET instrument, at 7110-km radius (740-km altitude). In order to obtain $\alpha(a)$ for $a > 7110$, an exponential extrapolation of $\alpha(a)$ based on information from $a < 7110$ is used. In order to avoid dealing with the singularity at the lower boundary of the integral, equation (5a) is rewritten as

$$\ln(n(a)) = -\frac{1}{\pi}\left[\alpha(a_{\text{int}})\ln\left(a_{\text{int}} + \sqrt{a_{\text{int}}^2 - a^2}\right) - \alpha(a)\ln(a) - \int_a^{a_{\text{int}}} \ln\left(a'^2 + \sqrt{a'^2 - a^2}\right)\frac{d\alpha(a')}{da'}da'\right] - \frac{1}{\pi}\int_{a_{\text{int}}}^\infty \frac{\alpha(a')}{\sqrt{a'^2 - a^2}}da' \qquad (5b)$$

where a_{int} is an intermediate value between a and ∞ and is normally chosen to be slightly larger than a. The

terms in brackets on the right-hand side of equation (5b) are the result of integration by parts.

In the ionosphere, the index of refraction is related to electron density via

$$n = 1 - 40.3 \times \frac{n_e}{f^2} , \qquad (6)$$

where n_e is the electron density per cubic meter and f is the operating frequency in hertz. Equations (2)-(6) constitute the essence of the radio occultation profiling technique as it applies to the ionosphere. In the next two sections we will examine bending and electron density profiles derived with this technique.

3. Ionospheric Effects on GPS Occulted Signals

Data examined in this section were taken on May 4-5, 1995. During this period (and for much of the GPS/MET experiment) the L1 and L2 phase measurements for the occulted link were recorded once every 10 s when the tangent point was above ~120-km altitude, and once every 20 ms (50-Hz rate) when the tangent point was below that height. This is because the GPS/MET experiment's primary goal is to sense the lower neutral atmosphere. Therefore results presented in this and the next section will reflect a rather coarse vertical resolution (~20-30 km) above ~120 km and a much finer vertical resolution (of order 1.5 km, corresponding to 1/2-s smoothing in the processing) below ~120-km altitude.

On the basis of Snell's law, the bending of the signal locally is in the direction of the refractivity gradient. In a general and approximate sense, the gradient of refractivity in the ionosphere is pointing upward above the F_2 peak and downward below that peak. Therefore the GPS signals will generally bend upward and downward above and below the F_2 peak, respectively. Examining the bending of the GPS L1 signal for 61 GPS/MET occultations that took place on May 4, 1995, we observe the following features (Figure 2):

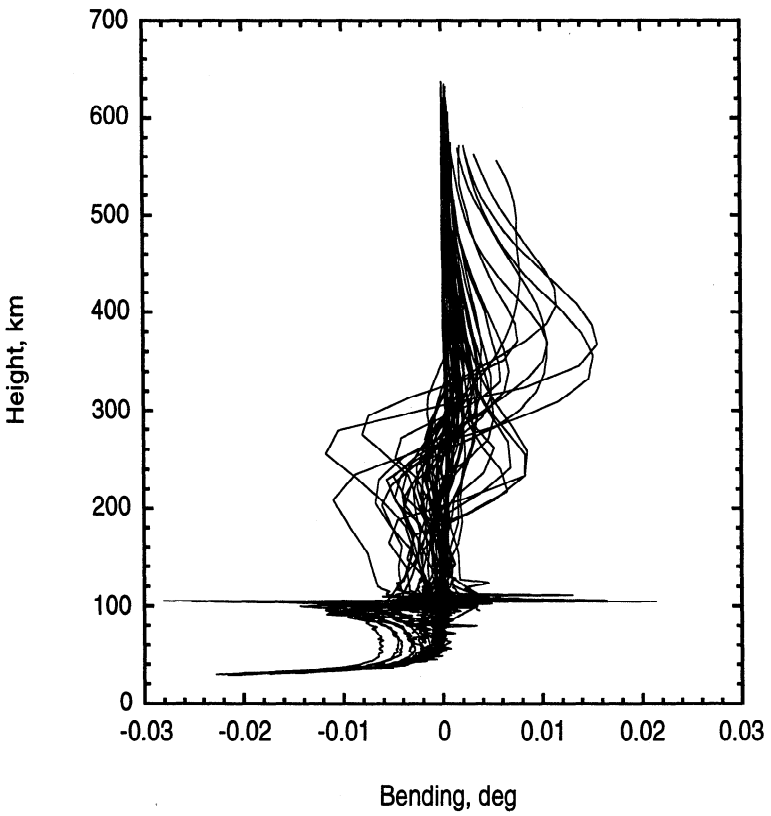

Figure 2. Bending induced by the ionosphere and neutral atmosphere on the L1 signal for 61 globally distributed occultations on May 4, 1995. Negative bending is defined to be toward the Earth's center.

1. The bending varies about 2 orders of magnitude between 0.0001 and 0.01 degrees (which cannot be seen from the scale of Figure 2), depending on local time and geographical location of the occultation. Since 1995 falls near a solar-minimum condition, the largest bending of Figure 2 can be an order of magnitude smaller than the corresponding solar-maximum condition.

2. The highest peak in bending, which is associated with the F_2 peak, varies in height between ~250 and 400 km, consistent with F_2 peak heights at different latitudes and local times.

3. With negative bending defined to be toward the Earth, the signal bends away from (toward) the Earth above (below) well-defined peaks in the ionosphere such as the F_2 and the E peaks. Since the bending of the signal depends on the gradient of the refractivity (which is vertical, to first order), one expects to see a change of sign in the bending as the tangent point samples through a peak.

4. Very sharp variations of bending are associated with sporadic E layers. The largest absolute bending for this particular day is ~0.03 degrees, which corresponds to the signal just descending below a sporadic E layer. The fact that the bending induced by the sporadic E is larger than that of the F_2 is due to the very short scale height associated with the sporadic E layer, which makes the refractivity gradient largest there.

5. The tails at the bottom end of all these curves start to grow in magnitude due to the neutral atmospheric bending which dominates below about 50-km altitude.

The most striking feature of these data is how sharp the signature is around the E (or sporadic E) layer. Even though determination of the magnitude of the E peak electron density might be obscured due to the overlaying layers and the assumption of spherical symmetry, the height of sharp E layer appears to be reasonably well determined. However, no definite conclusion regarding the accuracy of these heights can be drawn without further analysis and simulation accounting for the E layer horizontal variability and the effect of spherical symmetry assumption on the retrieval.

Bending of the L2 signal is a factor of 1.65 (equal to $(154/120)^2$, the square of the ratio of L1 to L2 frequencies) larger than for L1 (see equation (6)). This dispersive nature of the ionosphere causes the L1 and L2 signals to travel slightly different paths and therefore sample different regions (as indicated by the solid and dashed lines in Figure 1). This causes the tangent points of the two links to be at different heights in the atmosphere at a specific time. With the Abel inversion technique, the electron density profile and the height of the tangent point at a particular instant during the occultation can be solved for. Figure 3 shows an example of an electron density retrieval obtained from GPS/MET for an occultation taking place near 6°N latitude and 228°E longitude around 2004 UT of May 4, 1995 (the corresponding local time is 1104). Also shown on the figure is the separation between the L1 and L2 tangent points as a function of altitude. In the neighborhood of the F_2 peak, the relative positions of the two signals change due to changing direction of bending. Above the F_2 peak, since the bending is generally upward, the L2 tangent point will always be lower than the L1 tangent point The situation reverses when the signal tangent point is below the F2 peak. For this particular profile, the maximum separation is ~260 m corresponding to a maximum L1 bending of ~0.008°. The L1 and L2 separation scales linearly with the signals' bending, therefore one can expect separations that are 2 orders of magnitude smaller (as seen with the bending) or 1 order of magnitude larger during solar-maximum daytime. When the separation is of the order of a few kilometers, then the dual frequency approach of measuring TEC, which assumes that the two signals travel along the same raypath, will yield a small, but not insignificant, fractional TEC error. Moreover, a large separation of the two signals can be a limiting error for neutral atmospheric retrievals at altitudes above ~40 km [*Kursinski et al.*, 1997] unless higher-order corrections are applied to calibrate for the ionosphere.

We now turn our attention to some amplitude data obtained from GPS/MET. Figure 4 shows the flight receiver signal-to-noise ratio (SNR) of the L1 and L2 signals for four different occultations, where time = 0 corresponds to the start of high-rate data at about 120-km altitude for each occultation. The gradual decrease of SNR starting at about 30-40 s is due to significant atmospheric bending starting at about the tropopause. As the signal approaches the surface, it bends significantly (up to ~1°), defocuses, and finally disappears. Nearly half of the occultation displays a smooth steady SNR while the signal is in the ionosphere. Figure 4d is an example of one such smooth SNR. However, a good fraction of them (see Figures 4a, 4b, and 4c) show one or several sharp changes in SNR which can be attributed to sharp layers

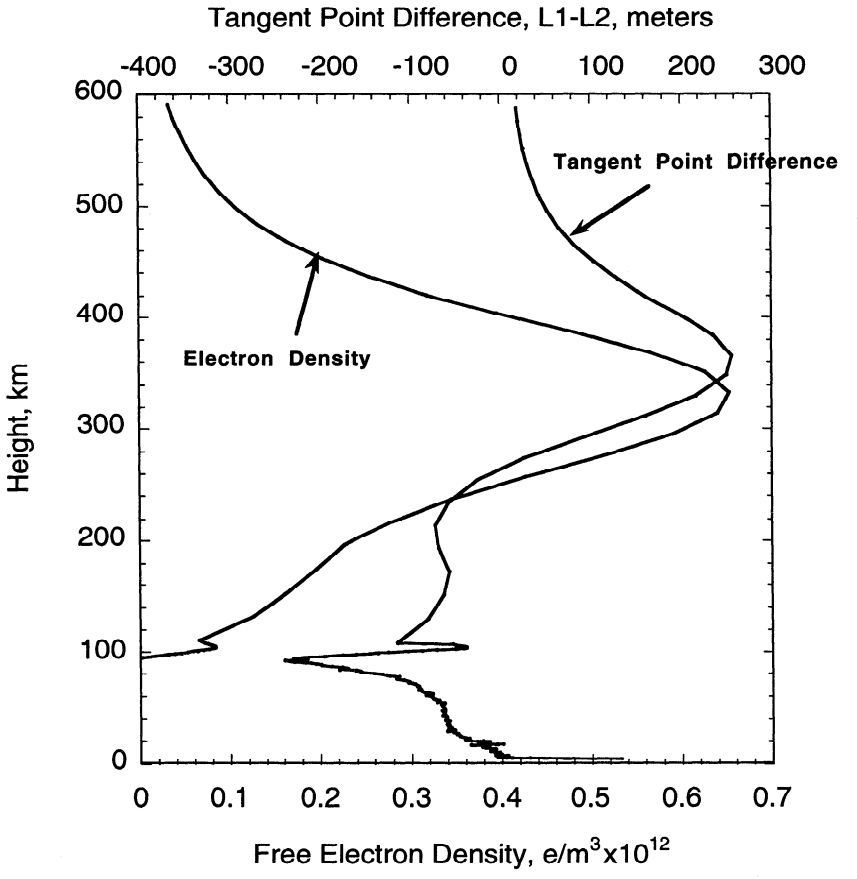

Figure 3. Electron density retrieved from occultation and the corresponding amount of L1 and L2 signal vertical separation at the tangent point.

(e.g., sporadic *E*) at the bottom of the ionosphere. That these scintillations are caused by the ionosphere and not the neutral atmosphere can be seen from the fact that the L2 SNR fluctuation is larger than that of L1, consistent with its lower carrier frequency.

The electron density profiles obtained with the Abel inversion corresponding to the occultations of Figure 4 are shown in Figure 5. Figures 5a, 5b, and 5c show one, several, and two sharp layers, respectively, at the bottom of the ionosphere. The sensitivity to ionospheric structures of very short vertical scales, such as sporadic *E*, is a consequence of the high vertical resolution characteristic of the GPS occultation limb viewing geometry. The theoretical vertical resolution of ionospheric profiles obtained from GPS-LEO occultations is set by the diffraction limit which corresponds to the first Fresnel zone diameter of ~1.5 km. However, a more practical limit on the vertical resolution for the ionosphere is introduced by horizontal structures which, if ignored, can alias into vertical structures. Therefore, no definite conclusion can be reached regarding the accuracy of the heights of these sharp layers without further studies.

4. Occultation Coverage and Electron Density Profiling

4.1. GPS/MET Coverage

As mentioned above, owing to the antenna field of view (±30°) and memory limitations on board the satellite, only 100-200 occultations per day are collected from the GPS/MET. The coverage obtained during 20 days of the mission (April 24 and 25, May 3 and 4, June 21-24 and 27-30, and July 1-7 of 1995) is shown in Figure 6a, where each occultation is represented by one point (corresponding to the location of the tangent point when it is at 100 km altitude). By contrast, the

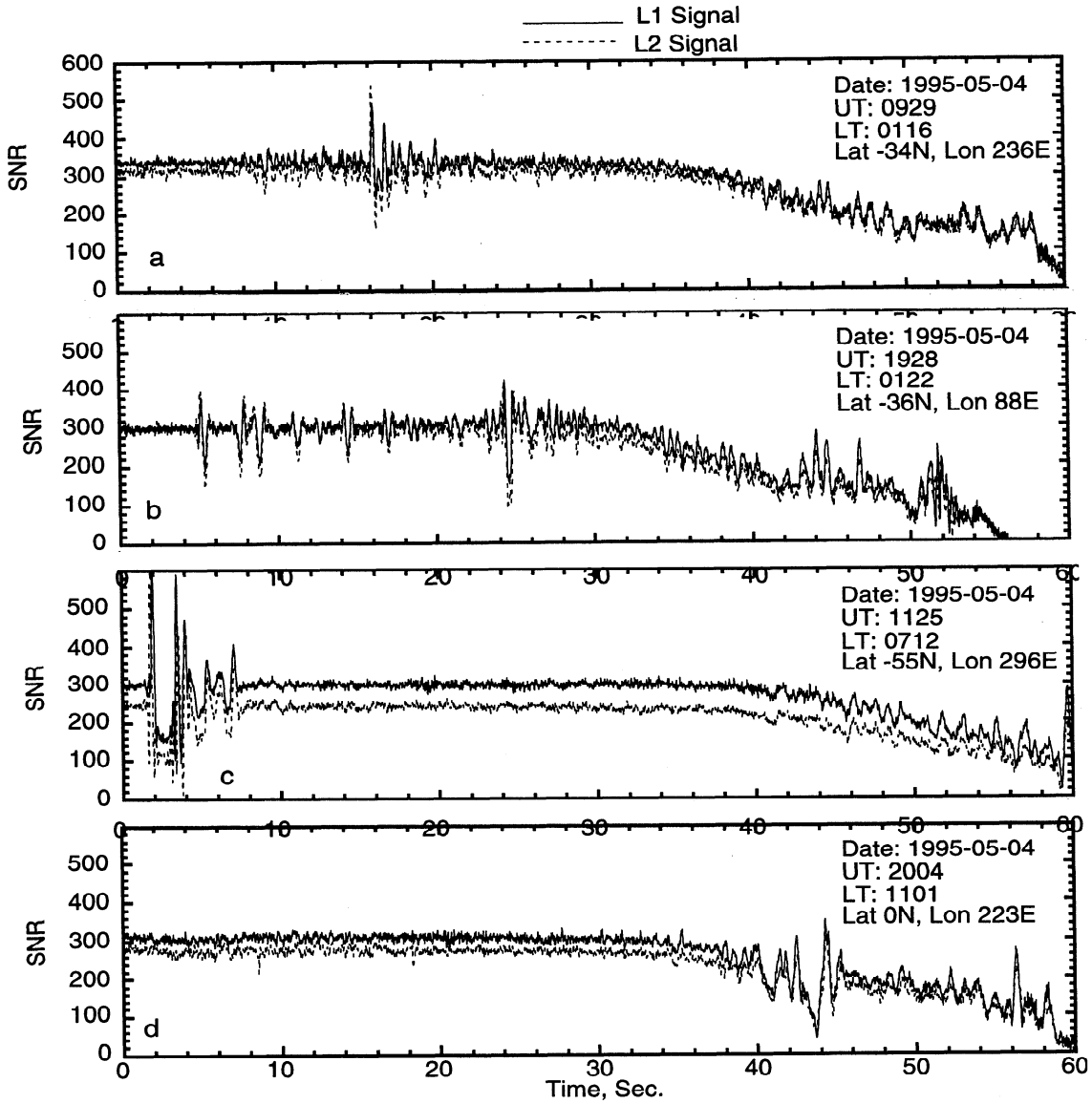

Figure 4. Instrumental signal-to-noise ratio as a function of time for L1 and L2 signals for four different occultations.

GPS/MET coverage for one day in Sun-fixed coordinate is shown in Figure 6b where each connected line corresponds to the ground projection of an occultation link when its tangent point (middle of the line) is at 100-km altitude. The ends of the line correspond to points on that same link at 400-km altitudes.

Since the coverage in Figure 6b is shown as a function of Sun-fixed longitude (0 Sun-fixed longitude corresponds to noon local time), and the occultations are scattered along the LEO orbit, the occultations are concentrated along the ground track of the GPS/MET satellite. At middle and low latitude the LEO samples the ionosphere at about the same latitude and local time for every revolution of the LEO orbit. This local time will precess slowly with the precession of the LEO orbit. For GPS/MET, it takes 110 days for a full precession of the satellite; therefore it takes half of this period to sample the Earth at all local times for middle and low latitude. On the other hand, at high latitude, the same 12-hour period is sampled for a given hemisphere (e.g., in Figure 6b the northern hemisphere is always sampled between noon and midnight local

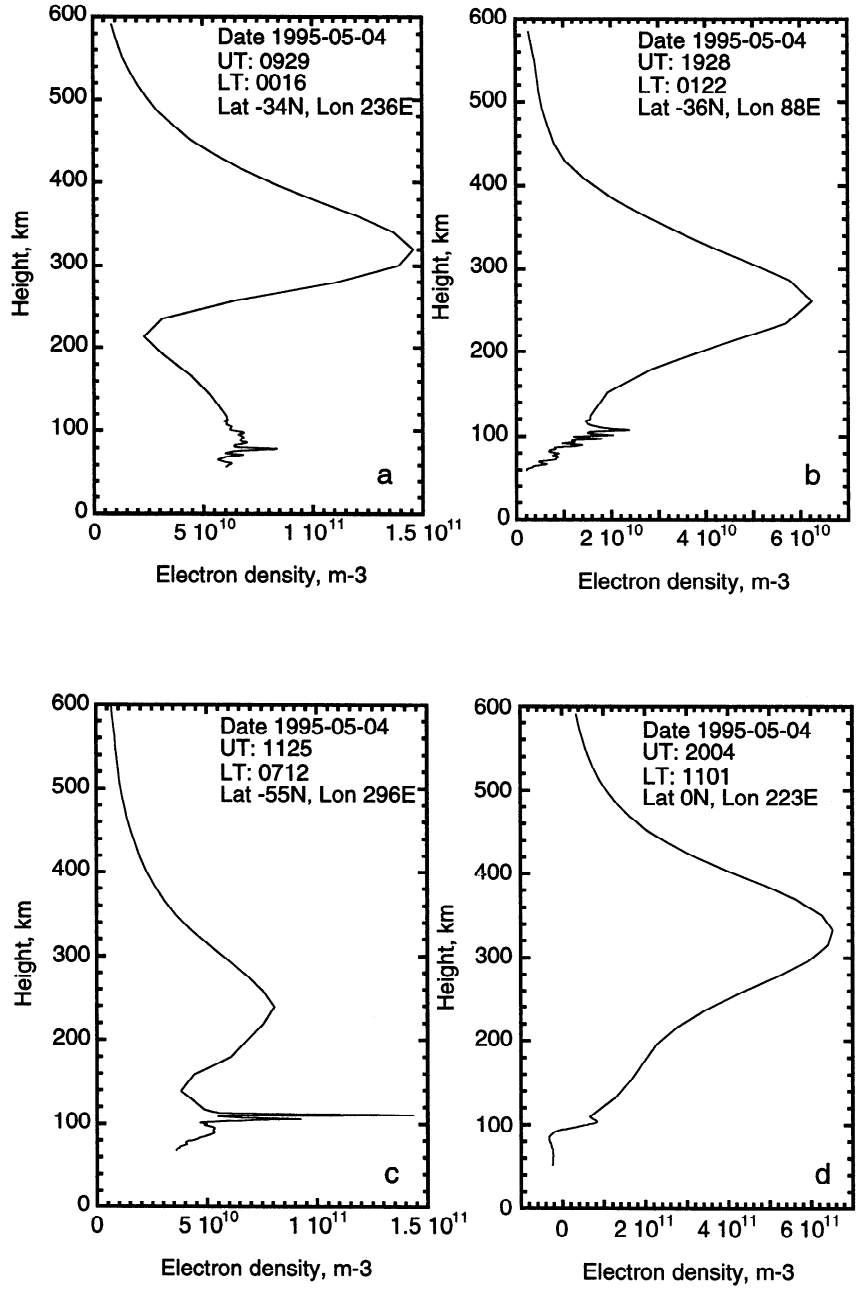

Figure 5. GPS/MET profiles of electron density corresponding to the occultations of Figure 4 and indicating the ability of GPS occultations to resolve sharp layers in the ionosphere.

time, whereas the southern hemisphere is sampled between midnight and noon local time). It takes half of the precession period to reverse the sampling geometry.

The width of the spread of occultations around the LEO track is determined by the width of the field of view of the receiving antenna and the distance to the limb. For a 740-km-altitude satellite (such as GPS/MET) the limb is about 3000-km away from the satellite. This implies that the tangent point of an occultation falls within a 3000 km radius from the

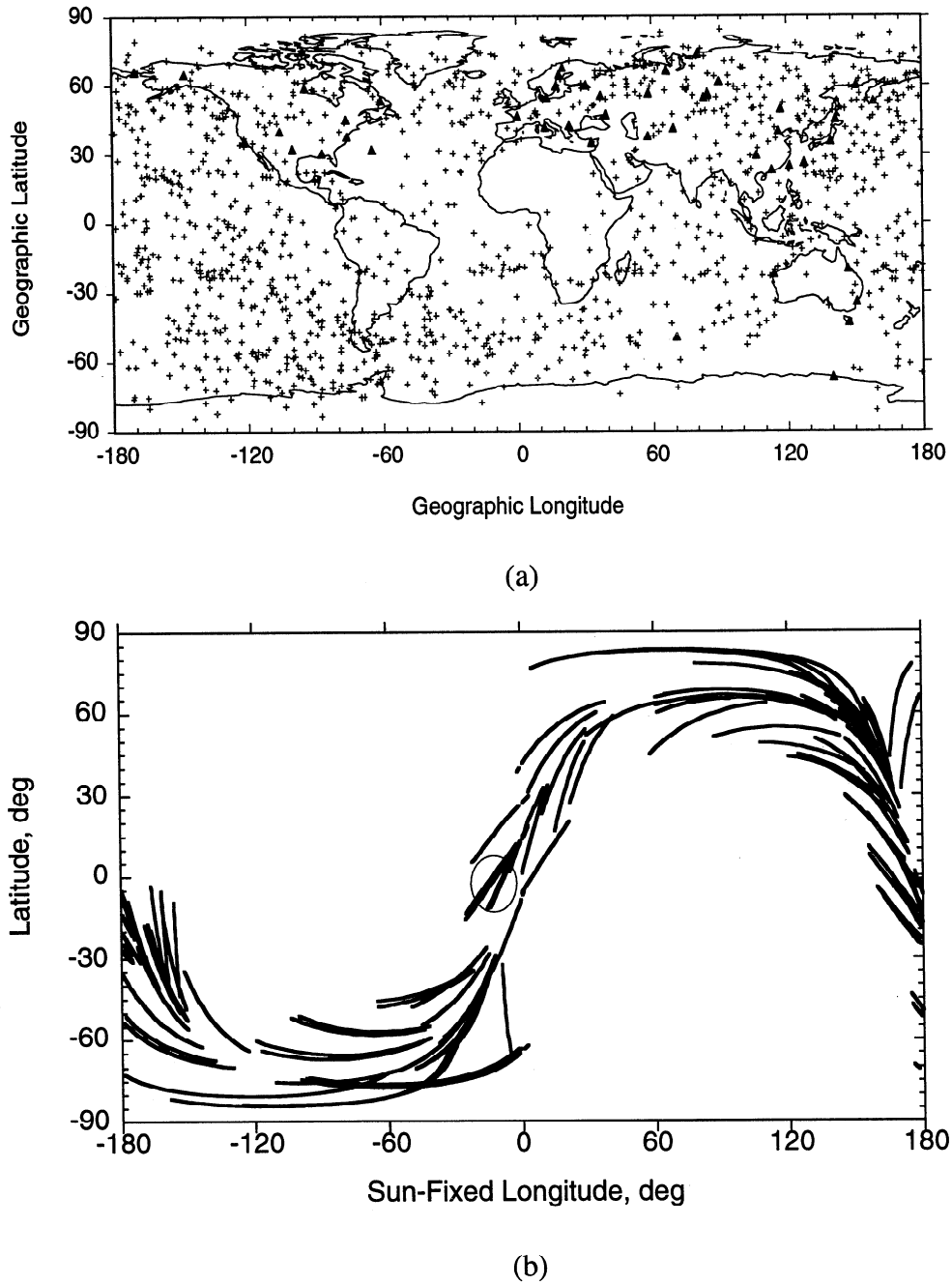

Figure 6. (a) GPS/MET coverage in geographic coordinates for 20 days (April 24 and 25, May 3 and 4, June 21-24 and 27-30, and July 1-7 of 1995). Each dot indicates the location of the tangent point of the occultation when it is at ~100 km altitude. The triangles indicate locations of ionosonde stations used in order to compare with N_mF_2 derived from GPS/MET. (b) GPS/MET coverage in Sun-fixed coordinates in 24 hours, May 4, 1995. Each connected line corresponds to the ground projection of an occultation link when the tangent point (middle of the line) is at 100-km altitude. The ends of the lines correspond to points on that same link at 400-km altitudes. At low latitude, the occultations sample roughly the same local time and same latitude every orbital revolution. The circle indicates four occultations corresponding to four consecutive orbital revolutions (~100 min apart); the corresponding profiles are shown in Figure 7a.

satellite trajectory during that occultation, setting an upper limit on the width of the spread of occultations around the LEO track to be ~±27 equatorial degrees.

4.2. Comparisons of GPS/MET Profiles With PIM

The reoccurrence of occultations at nearby local times and latitudes is illustrated by showing the retrievals of four equatorial occultations appearing at consecutive orbital revolutions, each taking place near noon local time. (These four occultations cross the circle in the middle of Figure 6b.) The electron density retrievals for these four occultations (using the Abel inversion) are shown in Figure 7a.

For comparisons, profiles obtained from the parameterized ionospheric model (PIM) [*Daniell et al.*, 1995] derived with input parameters suitable for the same day are also shown. Some of the main features to observe are (1) the ability to observe the E, F_1, and F_2 layers that are characteristic of the middle- and low-latitude daytime ionosphere; (2) the ability to observe the evolution of the ionosphere at the same local time and latitude every ~100 min (the GPS/MET orbital period) for middle- and low-latitude occultations; (3) except for the far-left profile shown in Figure 7a, the PIM reproduces F_2 peak densities and heights that are in reasonable agreement with the GPS/MET retrieval; (4) comparisons with the PIM are generally better below the F_2 peak than at the topside; (5) and the ability of both the model and the retrievals to reproduce the sharp decay of electron density at the bottom of the ionosphere. Other examples of GPS/MET retrieved profiles are shown for high latitude between dusk and midnight local time in Figure 7b. We note the low F_2 peak height, the near disappearance of the F_1 peak, and the very low peak density near midnight local time (far-right in Figure 7b). In contrast to the equatorial profiles the comparison with the PIM model appears to be more favorable at the topside than below the F_2 peak.

4.3. Comparisons of GPS/MET Profiles With ISR and Ionosonde

In order to assess the accuracy of the GPS/MET retrievals, coincidences of other types of data such as ionosondes or incoherent scatter radar (ISR) with GPS/MET occultations have been examined. Figure 8a shows a GPS/MET profile obtained on May 5, 1995, at about 0320 UT, with tangent points coordinates at about 41.9°N and 282.3°E (the tangent points for this occultation drifted from 40°N to 43.8°N and from 281.1°E to 283.6°E during the 4 min duration of the occultation). On the same figure are two ISR measurements of electron density obtained with a 640-μs pulse mode at about the same time and 20 min after the occultation. In Figure 8b the same GPS/MET profile is compared with an ISR profile obtained with a 320-μs pulse mode about 20 min after the occultation. Millstone Hill is located at 42.6°N and 288.5°E, which is about 6° east of the occultation location. The general agreement is fairly good. Discrepancies between the ISR and the occultation can be ascribed to several factors, including the spatial separation between the occultation and the ISR measurements, error introduced by the spherical symmetry assumption when doing the GPS/MET retrieval, and the lower vertical resolution of the ISR measurements.

A more extensive comparison of N_mF_2 derived from f_oF_2 ionosonde measurements and GPS/MET profiles has been performed, with results shown in Figure 9a. The comparison is between data obtained from a global network of ionosondes (Figure 6a) and GPS occultations that took place within 1 hour and ~1100-km radius (corresponding to 10 degrees) from the ionosonde stations. The points shown on the figure correspond to all the coincidences found for the 20-day period of Figure 6a. The middle line in Figure 9a corresponds to perfect agreement between these two measurements of N_mF_2. The upper and lower lines on the figure correspond to +20% and -20% deviation of GPS/MET derived N_mF_2 from the ionosonde N_mF_2, respectively. Differences in these two measurements are due to (1) error in the spherical symmetry assumption of the GPS/MET retrieval, (2) error in the ionosonde measurement, and (3) spatial and temporal mismatch between the occultation time and location and those of the ionosonde. In order to better quantify these errors, we examine the fractional difference in N_mF_2, defined as

$$\delta = \frac{N_mF_2(\text{GPS/MET}) - N_mF_2(\text{Ionosonde})}{N_mF_2(\text{Ionosonde})}, \quad (7)$$

as a function of the separation distance between the two measurement, shown in Figure 9b. There is an obvious growth in δ for larger separation distance. Limiting ourselves to measurements that are <600 km apart (36 measurements out of 99), Figure 10 shows a histogram of δ, which has a mean of 0.01, a standard deviation of 0.2, and a standard error in the mean of 0.03. The largest δ is 0.6.

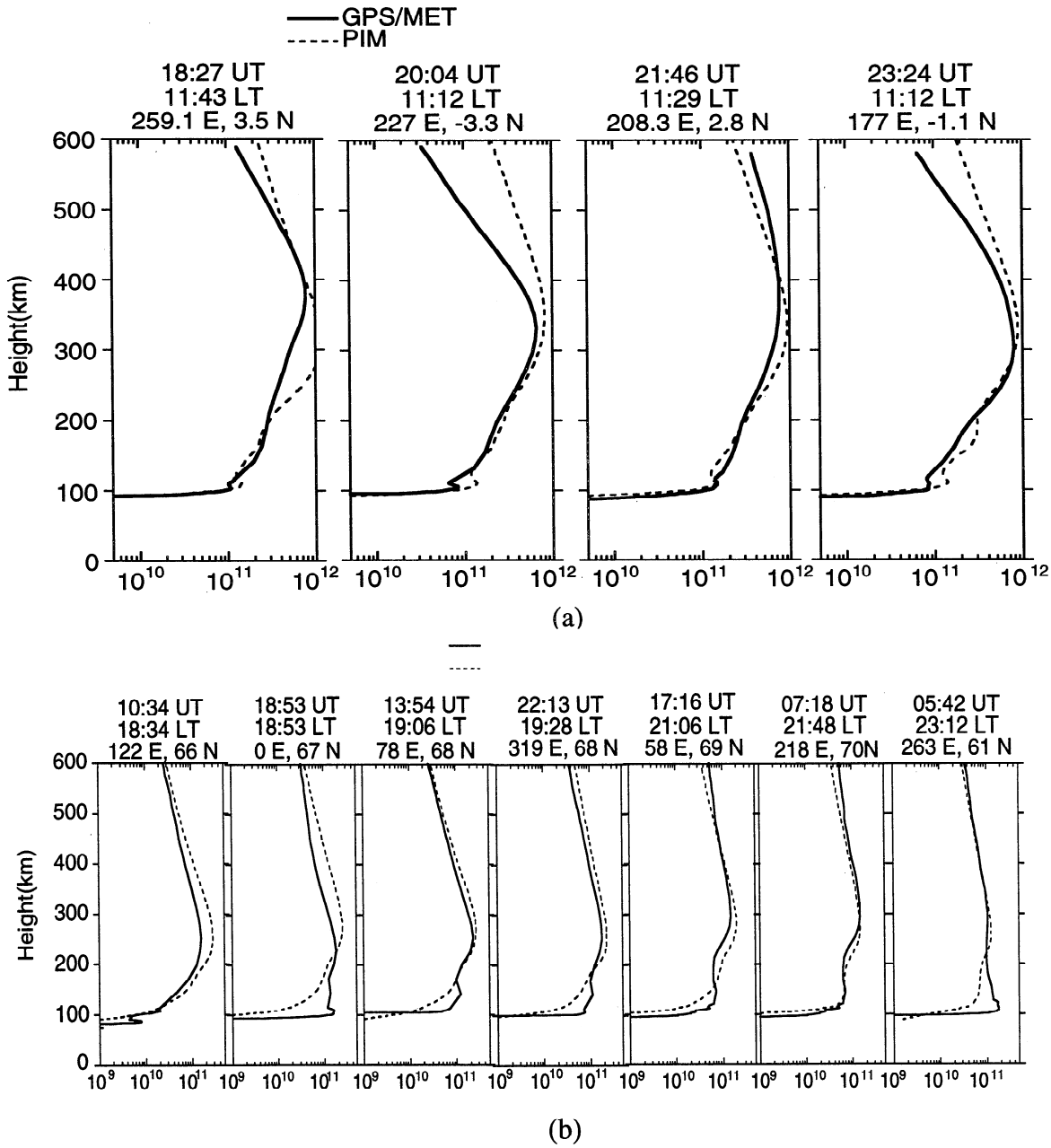

Figure 7. Examples of electron density profiles (e/m^3) obtained from GPS/MET and parameterized ionospheric model (PIM) for May 4, 1995: (a) low-latitudes profiles and (b) high-latitudes profiles. Indicated on the top of each profile are universal time, local time, latitude, and longitude of each occultation.

5. Discussion and Conclusion

GPS occultations have been shown to provide a new and complementary vantage point over ground based measurements for probing the ionosphere. In the work described herein we have chosen to process bending obtained from a single frequency, which is possible through modeling the geometry and calibration of the receiver and transmitter clocks in the data processing stage. Another approach, which is appropriate for

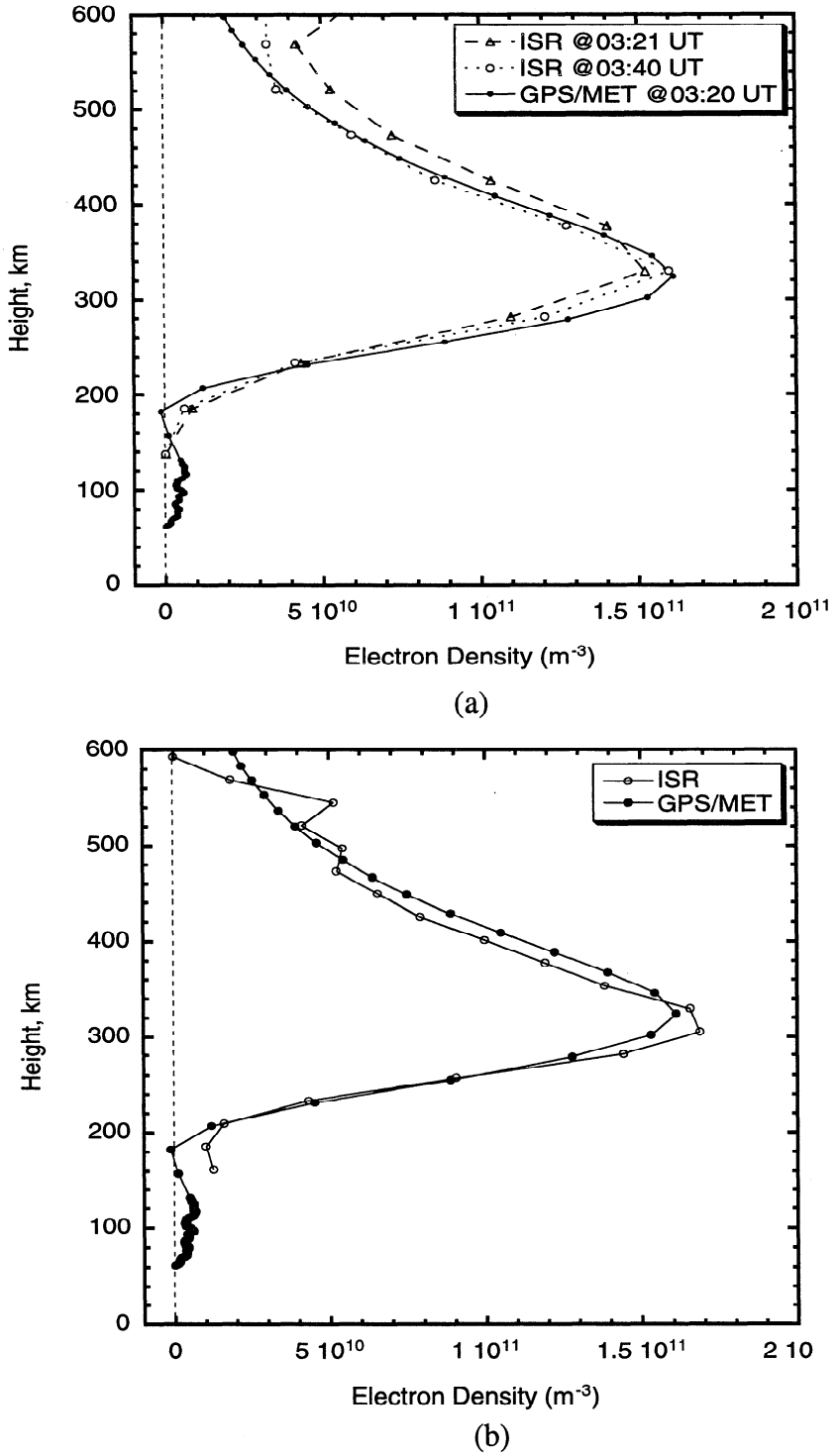

Figure 8. Comparisons of an electron density profile obtained from GPS/MET on May 5, 1995, 0320 UT, with nearby measurements from Millstone Hill incoherent scatter radar (ISR). (a) GPS/MET versus two ISR measurements with 640-μs pulse mode at 0321 UT and 0340 UT. (b) GPS/MET versus ISR measurements with 320-μs pulse mode at 0341 UT. The occultation tangent point is about 6^0 west and 1^0 south of Millstone Hill.

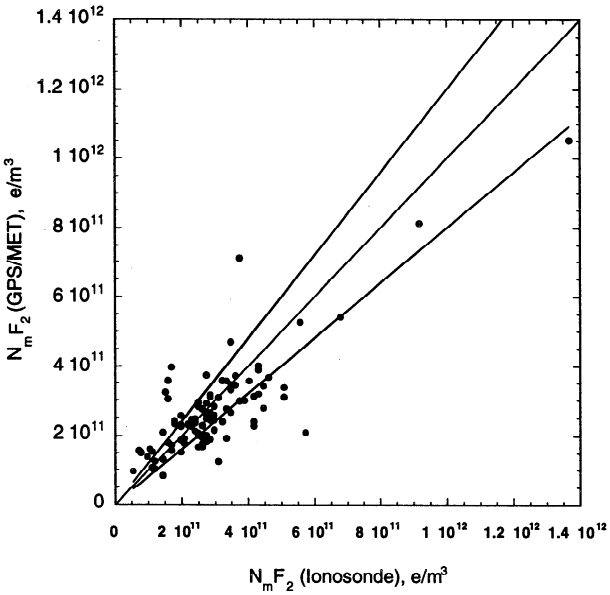

Figure 9a. A scatterplot of N_mF_2 derived from ionosonde measurements of f_oF_2, and GPS/MET electron density profiles, showing the degree of correlation between the two. The middle line corresponds to perfect correlation; the upper and lower lines bound the region of 20% deviation in the two measurements.

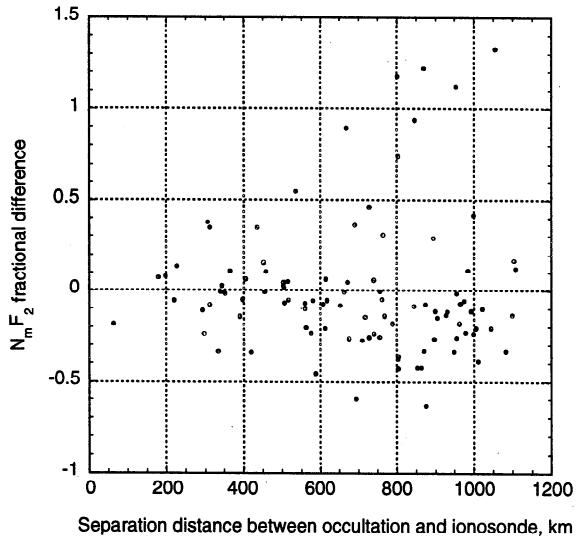

Figure 9b. The fractional difference between N_mF_2 derived from GPS/MET and the ionosonde (defined in equation (7)) as a function of the distance between the station and the tangent point of the occultation. Differences that are larger than ~0.5 can be attributed to the large distance between the station and the occultation.

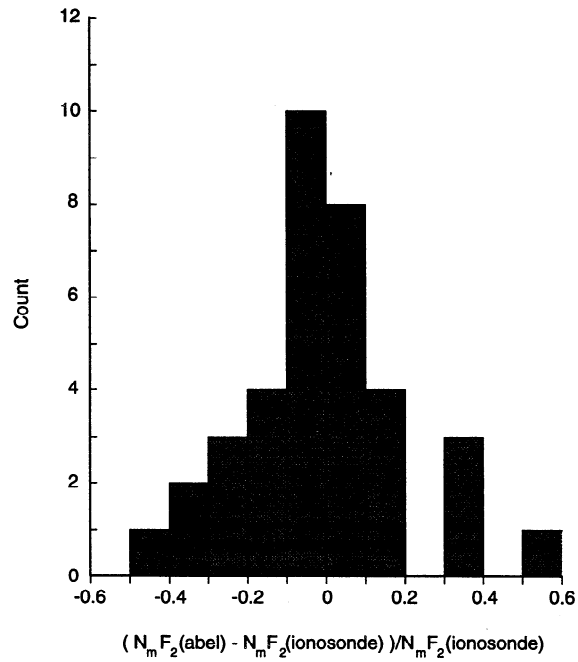

Figure 10. Histogram of the fractional difference between N_mF_2 derived from GPS/MET and the ionosonde for measurements within 1 hour and 600 km from each other. Average and standard deviation are 0.01 and 0.20, respectively. On the basis of this histogram, the two independent measurements of N_mF_2 agree to within 20% (1-sigma) and are essentially unbiased.

ground-based or uncalibrated space-based measurements, would be to process the combination L1-L2 (as done, for example, by *Leitinger et al.* [1997]); this directly isolates the ionospheric delay. This dual-frequency approach has the advantages of being much simpler in principle because it eliminates the need for precise orbits and for transmitter and receiver clocks calibration, which in turn eliminates the need for simultaneous ground measurements. This simplicity, however, is at the cost of lower precision due to the noise added by L2, especially under conditions when the Department of Defense anti-spoofing (AS) is turned on.

For the period analyzed (near solar minimum), bending in the ionosphere is of the order of 0.01° or less, with occasional stronger bending (up to 0.03°) occurring near sporadic E layers; a 0.01° of bending implies a separation between the L1 and L2 signals of ~350 m near the tangent point. At a period of solar maximum, these effects are expected to be an order of magnitude larger.

The strong vertical refractivity gradient at sporadic E layers causes strong scintillation and relatively large

bending, which makes this technique potentially very useful for detecting the existence of these layers and their heights. However, further analysis that considers the effect of the spherical symmetry assumption on the retrieved profile is needed to determine the accuracy of these heights.

We have evaluated the accuracy of N_mF_2 measurements based on GPS/MET profiles by comparing with nearby ionosondes, when available. On the basis of statistics presented in section 4 above, we can conclude that N_mF_2 independently derived from GPS/MET retrievals and ionosonde measurements agree to within 20% (at the 1-sigma level) and are essentially unbiased with respect to each other. This level of agreement is consistent with previous results [*Hajj et al.*, 1994], where a simulation experiment indicated that N_mF_2 accuracy can be expected to be in the range of 0-50%, depending on the degree of nonsphericity encountered in the ionosphere.

With the assumption of spherical symmetry used in the Abel transform, the peak electron density is overestimated or underestimated at the tangent point, depending on whether the ionosphere at that point is at a relative minimum or a relative maximum, respectively. Linear (or higher odd) power gradients in the horizontal distribution do not influence the retrievals when spherical symmetry is assumed, simply because these terms cancel when integrated across an occultation link; only even terms in the gradient survive and appear as errors in the retrievals. *Hajj et al.* [1994] have shown that a significant improvement can be made to the spherical symmetry assumption by making use of global ground maps of vertically integrated TEC measurements such as those computed by *Mannucci et al.* [1997] The idea introduced there was to impose a horizontal gradient at each layer identical to that of the TEC map and then solve for a scale factor for each layer. In this manner, each occultation is processed individually but without assuming a spherically symmetric ionosphere. Alternatively, and more powerfully, one can combine nearby occultations along with ground links in order to perform 3-D tomography of the ionosphere [*Høeg et al.*, 1995; *Hajj et al*, 1996; *Gorbunov et al.*, 1996; *Leitinger et al.*, 1997].

Appendix

Here we calculate the error in estimated bending due to setting the index of refraction to unity at the receiver's or transmitter's heights.

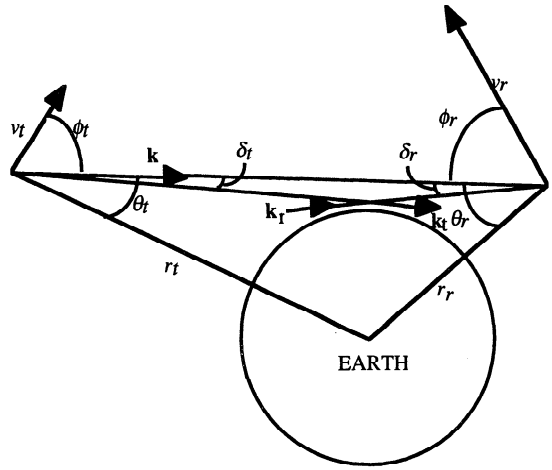

Figure A1. Geometry showing the direct line of sight between transmitter and receiver and the asymptotes of transmitted and received signals.

Consider the geometry of Figure A1 below, where the transmitting and receiving satellites are at radii r_t and r_r and travel with velocities $\mathbf{v}_t$ and $\mathbf{v}_r$ respectively . The signal is transmitted in the direction of $\mathbf{k}_t$ and received in the direction of $\mathbf{k}_r$. Here $\mathbf{k}$ is in the direction of the straight line connecting the transmitter and the receiver and corresponds to the direction that the signal would travel in vacuum. The extra Doppler shift caused by the intervening medium is then given by

$$\begin{aligned}\Delta f &= \frac{f}{c}\left(v_t\cos(\phi_t+\delta_t)+v_r\cos(\phi_r+\delta_r)\right)\\ &\quad -\frac{f}{c}\left(v_t\cos\phi_t+v_r\cos\phi_r\right)\\ &= -\frac{f}{c}\left(v_t\sin(\phi_t)\delta_t+v_r\sin(\phi_r)\delta_r\right)\end{aligned}, \qquad (8)$$

where the angles are defined in Figure A1. In addition, the formula of Bouguer [*Born and Wolf*, 1980], valid for spherically symmetric media, implies

$$n_t\sin(\theta_t-\delta_t)r_t = n_r\sin(\theta_r-\delta_r)r_r \qquad (9)$$

where n_t *and* n_r are the index of refraction at the transmitter and receiver, respectively. Equations (8) and (9) are used to solve for δ_r and δ_t, which correspond to the bending of the signal on each side of the occultation (see Figure A1). The total bending is the sum of these two terms.

In order to determine the error introduced by setting n_r and n_t to unity, we write equations (8) and (9) for $n_t = 1 + \varepsilon_t$ and $n_r = 1 + \varepsilon_r$ (denoting the solution δ_r and δ_t)

and then for $n_t = 1$ and $n_r = 1$ (denoting the solution δ_r' and δ_t') and then subtract the two sets of equations. This procedure, after expanding equations (8) and (9) to first order in δ_r ,δ_t and ignoring the small terms $\varepsilon_r\delta_r$ and $\varepsilon_t\delta_t$, leads to

$$v_t \sin(\phi_t)\Delta\delta_t + v_r \sin(\phi_r)\Delta\delta_r = 0, \quad (10)$$

and

$$\cos(\theta_t)\Delta\delta_t r_t + \varepsilon_t \sin(\theta_t) r_t = \cos(\theta_r)\Delta\delta_r r_r + \varepsilon_r \sin(\theta_r) r_r, \quad (11)$$

where

$$\Delta\delta_t = \delta_t' - \delta_t \quad \text{and} \quad \Delta\delta_r = \delta_r' - \delta_r$$

Solving equations (10) and (11), the error in the total bending $\Delta\alpha = \Delta\delta_t + \Delta\delta_r$ is given by

$$\Delta\alpha = \frac{\left(\varepsilon_r \sin(\theta_r) r_r - \varepsilon_t \sin(\theta_t) r_t\right)\left(v_r \sin(\phi_r) - v_t \sin(\phi_t)\right)}{r_t \cos(\theta_t) v_r \sin(\phi_r) + r_r \cos(\theta_r) v_t \sin(\phi_t)} \quad (12)$$

For GPS/MET geometry and a tangent height around 300 km, we have

r_r 7110 km;
r_t 26000 km;
v_r 7 km/sec;
v_t 3.8 km/sec;
θ_r 70°;
θ_t 15°;
ϕ_r 20°;
ϕ_t 75°.

Let $N_e(h_{\mathrm{LEO}})$ be the electron density at the receiver's height; then $\varepsilon_r = (n-1) = -40.3 N_e(h_{\mathrm{LEO}})/f^2$ (N_e is per cubic meter, f is the radio frequency in hertz). At the GPS height we set $\varepsilon_t \approx 0$ since the electron density is vanishingly small. Then, equation (12) reduces to

$$\Delta\alpha \equiv \alpha_{\mathrm{estimated}} - \alpha_{\mathrm{true}} = 0.123 \times \frac{40.3}{f^2} N_e(h_{\mathrm{LEO}}), \quad (13)$$

For $N_e(h_{\mathrm{LEO}}) = 10^{10}$ m^{-3} and f =1.57542 GHz, we get $\Delta\alpha = 1.1\times10^{-6}$ degrees.

Therefore, by ignoring the deviation of n from unity, we are overestimating the true bending caused by the ionosphere as derived from the GPS carrier phase measurements. (Note that we would be underestimating the bending by the same amount if we were to derive it from the GPS pseudorange measurements since ε_r would have the opposite sign.) Of importance is the bending error relative to the total bending. This fractional error can be approximated by using the following simple model for the ionosphere. Let

$$N_e(h) = N_{\max} \exp\left(-\frac{h - h_{\max}}{H}\right) \quad h > h_{\max}$$

0 otherwise,

where $h_{\max}$ and $N_{\max}$ correspond to the peak height and peak density respectively; and H is the free electron density scale height. Then, to a good approximation, the total bending for a link with a tangent height $h > h_{\max}$ is given by [*Melbourne et al.*, 1994, p. 47]

$$\alpha(h) = \sqrt{\frac{2\pi R_{\max}}{H}} \frac{40.3}{f^2} N_{\max} \exp\left(-\frac{h - h_{\max}}{H}\right), \quad (14)$$

where $R_{\max} = h_{\max}$ + radius of Earth. The fractional bending error is then given by

$$\frac{\Delta\alpha}{\alpha}(h) = \frac{0.123}{\sqrt{\frac{2\pi R_{\max}}{H}}} \exp\left(-\frac{h_{\mathrm{LEO}} - h}{H}\right), \quad (15)$$

For h_{LEO} = 740 km, $R_{\max}$ = 6670 km, H = 70 km, we get

$$\frac{\Delta\alpha}{\alpha}(h) = 0.005 \exp\left(-\frac{h_{\mathrm{LEO}} - h}{H}\right).$$

On the basis of this exponential model and the GPS/MET geometry, bending is overestimated by less than 0.5% of the true one. In order to estimate the corresponding error in electron density, we use the differential form of the Abel transform integral (equation (5a)), which can be written as

$$\frac{\Delta n}{n} = -\frac{1}{\pi} \int_a^\infty \frac{\Delta\alpha}{\alpha} \frac{\alpha}{\sqrt{a'^2 - a^2}} da', \quad (16)$$

using equation (15) in (16), it is easy to establish that

$$\frac{(N_e)_{\mathrm{estimated}} - (N_e)_{\mathrm{true}}}{(N_e)_{\mathrm{true}}} \le \frac{0.123}{\sqrt{\frac{2\pi R_{\max}}{H}}} \approx 0.005, \quad (17)$$

This implies that the derived electron density is overestimated by no more than 0.5% of the true density.

Acknowledgments. We thank Mike Exner of UCAR for providing the GPS/MET flight data. We thank John Foster for providing the Millstone Hill ISR data. Ionosonde data were provided by the National Geophysical

Data Center. This research was performed at the Jet Propulsion Laboratory, California Institute of Technology, under the JPL Director's Research Discretionary Fund with partial funding from the National Science Foundation.

References

Born, M., and E. Wolf, *Principles of Optics*, 6th ed., Pergamon, Tarrytown, N. Y., 1980.

Daniell, R. E., L. D. Brown, D. N. Anderson, M. W. Fox, P. H. Doherty, D. T. Decker, J. J. Sojka, and R. W. Schunk, Parameterized ionospheric model: A global ionospheric parameterization based on first principles models, *Radio Science, 30*(5), 1499-1510, 1995.

Decker, D. T., D. N. Anderson, R. M. Campbell, and P. H. Doherty, Simulations of GPS/MET ionospheric observations (abstract), *Eos Trans. AGU, 77*(46), Fall Meet. Suppl., F142, 1996.

Fjeldbo, G. F., V. R. Eshleman, and A. J. Kliore, The neutral atmosphere of Venus as studied with the Mariner V radio occultation experiments, *Astron. J., 76,* 123-140, 1971.

Gorbunov, M. E., S. V. Sokolovsky, and L. Bengtsson, Space refractive tomography of the atmosphere: Modeling of direct and inverse problems, *Rep. 210,* Max-Planck-Inst. für Meteorol., Hamburg, F. R Germany, August 1996.

Gurvich, A. S. and T. G. Krasil'nikova, Navigation satellites for radio sensing of the Earth's atmosphere, *Sov. J. Remote Sensing,* 7, 1124-1131, 1990.

Hajj, G. A., R. Ibanez-Meier, E. R. Kursinski, and L. J. Romans, Imaging the ionosphere with the Global Positioning System, *Int. J. Imaging Syst. Technol., 5,* 174-184, 1994.

Hajj, G. A., E. R. Kursinski, W. I. Bertiger, S. S. Leroy, and J. T. Schofield, Sensing the atmosphere from a low-Earth orbiter tracking GPS: Early results and lessons from the GPS/MET experiment, in *Proceedings of ION-GPS 95, The 8th International Technical Meeting of The Satellite Division of The Institute of Navigation*, pp. 1167-1174, Alexandria, Va., 1995.

Hajj, G. A., L. Romans, W. Bertiger, R. Kursinski and T. Mannucci, Imaging the ionosphere with GPS/MET, paper presented at the URSI GPS/MET Workshop, Tucson, Ariz., Feb. 21-24, 1996.

Høeg, P., A. Hauchecorne, G. Kirchengast, S. Syndergaard, B. Belloul, R. Leitinger, and W. Rothleitner, Derivation of atmospheric properties using a radio occultation techniques, *ESA/ESTEC Contr. Rep. 11024/94/NL/CN, DMI Sci. Rep. 95-4*, edited by P. Høeg and S. Syndergaard, Danish Meteorol. Inst., Copenhagen, 1995.

Kursinski, E. R, et al., Initial results of radio occultation observations of Earth's atmosphere using the Global Positioning System, *Science, 271,* 1107-1110, 1996.

Kursinski, E. R., G. A. Hajj, J. T. Schofield, R. Linfield and K. R. Hardy, Observing Earth's atmosphere with radio occultation measurements using the Global Positioning System, *J. Geophys. Res., 102*(D19), 23,429-23,465, 1997.

Leitinger, R., H.-P. Ladreiter, and G. Kirchengast, Ionosphere tomography with data from satellite reception of Global Navigation Satellite System signals and ground reception of Navy Nav Satellite System signals, *Radio Sci., 32*(4), 1657-1669, 1997.

Leroy, S., The Measurement of geopotential heights by GPS radio occultation, *J. Geophys. Res., 102*(D6), 6971-6986, 1997.

Mannucci, A. J., B. D. Wilson, D. N. Yuan, C. M. Ho, U. J. Lindqwister, and T. F. Runge, A global mapping technique for GPS-derived ionospheric total electron content measurements, *Radio Sci.*, in press, 1997.

Meehan, T. K., et al., The TurboRogue GPS receiver, paper presented at the 6th International Geodetic Symposium on Satellite Positioning, Def. Mapping Agency, Columbus, Ohio, March 17-20, 1992.

Melbourne, W. G., E. S. Davis, C. B. Duncan, G. A. Hajj, K. R. Hardy, E. R. Kursinski, T. K. Meehan, L. E. Young, and T. P. Yunck, The application of spaceborne GPS to atmospheric limb sounding and global change monitoring, *JPL Publ. 94-18,* April 1994.

Tricomi, F. G., *Integral Equations*, Dover, Mineola, N. Y., 1985.

Tyler, G. L., Radio propagation experiments in the outer solar system with Voyager, *Proc. IEEE, 75,* 1404-1431, 1987.

Ware, R., et al., GPS sounding of the atmosphere from low earth orbit: Preliminary results, *Bull. Am. Meteorol. Soc., 77*(1), 19-40, 1996.

Yunck, T. P., G. F. Lindal, and C. H. Liu, The role of GPS in precise earth observation, paper presented at the IEEE Position, Location and Navigation Symposium, Orlando, Fl., Nov. 29-Dec. 2, 1988.

G. Hajj and L. Romans, Jet Propulsion Laboratory, 4800 Oak Grove Drive, Pasadena, CA. 91109, USA. (email: hajj@cobra.jpl.nasa.gov; ljr@cobra.jpl.nasa.gov)

(Received May 23, 1997; revised October 31, 1997; accepted November 5, 1997.)